NON-LINEAR FLUTTER ANALYSIS OF LABYRINTH SEALS

Roque Corral *
School of Aeronautics and Space
Universidad Politécnica de Madrid
28040 Madrid, Spain
e-mail: roque.corral@upm.es

Michele Greco †
School of Aeronautics and Space
Universidad Politécnica de Madrid
28040 Madrid, Spain
e-mail: michele.greco@upm.es

Luis Matabuena
Faculty of Aerospace Enginering
Technical University of Delft
2628 Delft, Netherlands
e-mail: J.L.MatabuenaSedano
@student.tudelft.nl

ABSTRACT

A simple nonlinear model to describe labyrinth seal flutter has been developed to assess the aeromechanic stability of straight-through labyrinth seals subjected to large gap variations. The model solves the one-dimensional integral mass, momentum, and energy equations of the seal for a prescribed motion numerically until a periodic state is reached. The model accounts for the effect, previously neglected, of high clearance variations on the stability. The results show that when the vibration amplitudes are small, the work-per-cycle coincides with the prediction of the Corral and Vega model (2018, "Conceptual Flutter Analysis of Labyrinth Seals Using Analytical Models. Part I: Theoretical Background", ASME J. Turbomach.140(10), pp. 121006) and Corral et al. (2021, "Higher-Order Conceptual Model for Seal Flutter", ASME J. Turbomach. 143(7), pp.071006), but for large vibration amplitudes nonlinearities alter the stability limit. In realistic cases, when the discharge time of the seal is much longer than the vibration period, the nonlinear effects are significant and tend to increase the unstable range of operating conditions. Furthermore, seals supported either on the high-pressure or low-pressure sides, stable for small vibration amplitudes, can destabilise when the vibration amplitude increases. The linear stability, though close in many situations to the nonlinear threshold, is not conservative, and attention must be paid to nonlinear effects.

INTRODUCTION

Labyrinth seals are extensively used in turbomachinery to control the leakage flow between rotating and stationary components. The most popular configurations are the straight-through, the stepped, and the staggered labyrinth seals. They are commonly used in the secondary air system to supply cooling air and to prevent the ingestion of hot gas from the mainstream to the turbine disks. They are also used to minimize the leakage flow between the blade tip and the casing. Labyrinth seals are composed of a series of cavities connected by constrictions where the flow is forced to pass through. The acceleration through the clearances generates kinetic energy, which is dissipated in the following cavity. This process produces losses reducing the leakage flow. For many years most of the studies regarding labyrinth seals have been driven by efficiency reasons, and the focus was on the seal steady flow characteristics. Even though simplified leakage flow models (see [1]) are still widely used in the industry.

The first pioneering studies conducted by Alford showed that seals are also a source of aeroelastic instabilities [2, 3, 4]. Afterwards, Lewis [5] conducted experimental analysis and observations on fractured seals revealing that seal flutter represents a critical issue of modern aero-engines. The first analytical model for seal flutter has been proposed by Ehrich [6]. His model was two-dimensional, and the stability was based on the torsion center location and the geometry of the seal. Later, in 1981 Abbot [7] released his model taking into account the circumferential perturbations. He introduced the ratio between the acoustic resonance and the natural frequency of the seal. The stability criterion, inconsistent with Ehrich's one, outlines that the stability is determined by two parameters: the ratio between the acoustic

*Professor at the Department of Fluid Dynamics and Aerospace Propulsion of the School of Aeronautics and Space, Universidad Politecnica Madrid
†Corresponding Author

resonance and the natural frequency of the seal and the support location.

Recently, Corral and Vega [8, 9] proposed a new comprehensive model for seal flutter. The model provides an expression for the work-per-cycle involving three dimensionless parameters, two of which completely new, to define the stability map of the seal. All the results of the classical analytical models are recovered and conciliated. The results were also extended to stepped seals [10]. Moreover, it has been identified that the tip labyrinth seal has an outstanding effect on the stability of shrouded turbine rotor blades [11]. CFD analyses were compared with the prediction of the Corral and Vega (CV) model, corroborating the stabilising effect predicted analytically. Recently, a new formulation of the baseline Corral and Vega model [8, 9] accounting for non-isentropic perturbations has been proposed [12]. The model redefines the dimensionless parameters described in [8, 9] and outlines a more general stability map of the seal. The high sensitivity of the seal stability to differential gapping and the role of the effective gaps and the carry-over coefficient have been addressed recently [13]. The stability trends outlined analytically have been validated numerically in [14, 13] by using a linearized Navier-Stokes solver.

Fins clearance changes with flight conditions and the rotor vibrations can cause radial displacements leading to instability issues. Ideally, the teeth and the casing are non-contacting, but when the instability sets in, this non-contacting nature is hard to maintain. It is not uncommon that the seal gap for some instants becomes very small and often even close. In this context, the flow variation on the seal cavity can be large compared with the design condition, suggesting that it can play an relevant role in its stability. All the analytical approaches to the seal flutter previously described are based on the use of linearized models considering that the fin displacements are small compared to the gap, therefore the impact of the nonlinearities on the stability of labyrinth seals has not been investigated.

This paper explores the aeromechanic stability of labyrinth seals for large variations of the seal gap. Firstly the analytical approach is introduced. Then the numerical integration of a reduced-order model is described, exploring the parameters involved in the formulation by varying the vibration amplitude. The impact of the nonlinearities on the stability is studied by considering first a simplified model neglecting the perturbations on the azimuthal direction. Although the engineering interest of this case is limited, it is important to understand the impact of the high vibration amplitudes on stability. Subsequently, the higher nodal diameter cases are introduced. The non-dimensional work-per-cycle has been compared with the linear formulation described in [12], highlighting the effect of the large gap variations in a wide range of operating conditions. Finally, the nonlinear stability map of a realistic case is compared with the linear stability limit, and some conclusions are drawn.

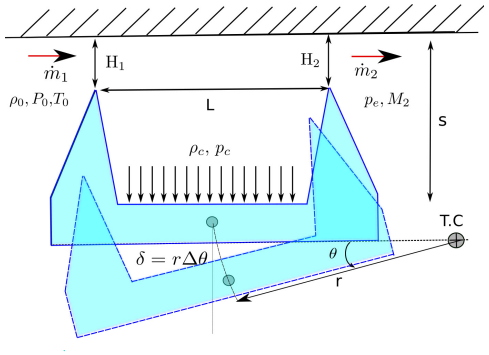

FIGURE 1. SKETCH OF A SIMPLIFIED LABYRINTH SEAL AND NOMENCLATURE

GOVERNING EQUATIONS

The model solves the semi-integral form of the mass, momentum and energy equations for the inter-fin cavity volume per unit length in the circumferential direction, $V_{c,2D}$,

$$\frac{\partial(V_{c,2D}\mathbf{U})}{\partial t} + \frac{\partial(V_{c,2D}\mathbf{h})}{\partial z} = \dot{m}_1\mathbf{f}_1 - \dot{m}_2\mathbf{f}_2 + \mathbf{Q} \tag{1}$$

where

$$\mathbf{U} = \begin{pmatrix} \rho_c \\ \rho_c v_\theta \\ \rho_c E_c \end{pmatrix}, \mathbf{h} = \begin{pmatrix} \rho_c v_\theta \\ p_c + \rho_c v_\theta^2 \\ \rho_c v_\theta h_{0c} \end{pmatrix} \tag{2}$$

are the vector of conservative variables, and the flux in the $z-$direction, and a source term, respectively. The fluid density ρ_c, circumferential velocity v_θ, static pressure p_c, total internal energy $E_c = c_v T + \frac{1}{2}v_\theta^2$, and total enthalpy $h_{0c} = c_p T + \frac{1}{2}v_\theta^2$, represent the spatially averaged properties of the cavity respectively, and $\dot{m}_1$ and $\dot{m}_2$ the inlet and outlet mass flows. The source term contributions

$$\mathbf{f} = \begin{pmatrix} 1 \\ v_\theta \\ h_{0c} \end{pmatrix}, \mathbf{Q} = \begin{pmatrix} 0 \\ p_c(V_{c,2D})_z \\ -p_c(V_{c,2D})_t \end{pmatrix} \tag{3}$$

represent the axial fluxes and the work of the cavity pressure in a varying volume (see [12] for further details).

Figure 1 shows the seal geometry and nomenclature used for the derivation of the model. In Fig. 1 the flow moves from the high-pressure side (HPS) on the left to the low-pressure side (LPS) on the right of the sketch, then $h_{0,1}$ is the total enthalpy in the HPS outer cavity, i.e. $h_{0,1} = h_0$, and $h_{0,2}$ is the spatially averaged total enthalpy in the seal cavity, $h_{0,c}$. It is well-known that in straight-through labyrinth seals, the kinetic energy generated in the inlet gap is not dissipated in the inter-fin cavity completely, and part of it is recovered in the downstream knife, depending on the seal geometry and the operating condition. This mechanism, which has been retained in [13], can change the stability of the seal considerably. The flow through the knife-seal is assumed quasi-stationary since the characteristic length of the inlet and outlet

gaps of the inter-fin seal cavity, H_1 and H_2 respectively, and their thicknesses are much smaller than the characteristic size of the inter-fin cavity, L, and therefore the fin through-flow time is much smaller than the cavity discharge time (The time that the seal would take to discharge through the exit gap with no incoming mass-flow). Under this assumption the kinetic energy recovered on the downstream fin is low as described in [13], therefore for the sake of simplicity it will be assumed that the effective total pressure in the exit fin is $p_{0,2} = p_c$. Moreover, the model also assumes that all the processes are adiabatic and that the work added to the inter-fin cavity by the windage and the seal vibration is negligible.

For an ideal gas, the non-dimensional quasi-steady dimensionless mass-flows through the gaps, $\bar{\dot{m}_1}$, and $\bar{\dot{m}_2}$, can be expressed as a function of the ratio of the inlet total pressure, and the discharge static pressure, $\pi_i = P_{0,i}/p_i$, as:

$$\bar{\dot{m}_1} = \frac{\dot{m}_1\sqrt{R_g T_0}}{p_0 A_1} = \pi_1^{-\frac{\gamma+1}{2\gamma}}\sqrt{\frac{2\gamma}{\gamma-1}\left(\pi_1^{\frac{\gamma-1}{\gamma}}-1\right)} = f(\pi_1), \quad (4)$$

$$\bar{\dot{m}_2} = \frac{\dot{m}_2\sqrt{R_g T_{0,c}}}{p_{0,c} A_2} = \pi_2^{-\frac{\gamma+1}{2\gamma}}\sqrt{\frac{2\gamma}{\gamma-1}\left(\pi_2^{\frac{\gamma-1}{\gamma}}-1\right)} = f(\pi_2) \quad (5)$$

where T_0, p_0, and $T_{0,c}(t)$, $p_{0,c}(t)$ are the inlet and the cavity spatially averaged total temperatures and pressures respectively. The dimensionless mass flows are a function only of the gap Mach numbers or the pressure ratios, $\pi_1 = p_0/p_c$ and $\pi_2 = p_{0,c}/p_e$, where p_e is the downstream static pressure.

The volume, $V_{c,2D}(t)$, and the gaps, $A_1(t)$ and $A_2(t)$, of the seal undergo a harmonic variation of angular velocity ω, which is directly related to the mode-shape. Using the following dimensionless variables

$$\tilde{\rho}_c = \frac{\rho_c}{\rho_0}, \tilde{p}_c = \frac{p_c}{p_0}, \tilde{T}_c = \frac{T_c}{T_0}, \tilde{v}_\theta = \frac{v_\theta}{\sqrt{\gamma p_0/\rho_0}}, \tilde{V}_c = \frac{V_{c,2D}}{V_{c,0}}, \quad (6)$$

$$\tilde{\dot{m}} = \frac{\dot{m}}{A_0\sqrt{\rho_0 p_0}}, \tilde{A}_j = \frac{A_j}{A_0}, \tilde{z} = \frac{ND\,z}{R}, \tau = \omega t$$

where the sub-index 0 refers to the total conditions upstream of the seal. The dimensionless governing equations become

$$\Omega_{NL}\left[\frac{\partial(\tilde{V}_c\tilde{\mathbf{U}})}{\partial\tau} - \tilde{\mathbf{Q}} + \frac{1}{St}\frac{\partial(\tilde{V}_c\tilde{\mathbf{h}})}{\partial\tilde{z}}\right] = \tilde{\dot{m}}_1\tilde{\mathbf{f}}_1 - \tilde{\dot{m}}_2\tilde{\mathbf{f}}_2 \quad (7)$$

where $\tilde{\mathbf{U}}$, $\tilde{\mathbf{h}}$ and $\tilde{\mathbf{f}}$ are the vectors of dimensionless conservative variables and fluxes, respectively, and

$$\tilde{\dot{m}}_1 = \tilde{A}_1(\tau)\,g(\tilde{p}_c) \text{ and } \tilde{\dot{m}}_2 = \tilde{A}_2(\tau)\,\frac{\tilde{p}_c}{\tilde{T}_{0,c}^{1/2}}\,g(\tilde{p}_c\pi_T)$$

the dimensionless mass-flows, and $g = \gamma^{-1/2} f$ a redefined function for the sake of concisness.The dimensionless parameter

$$\Omega_{NL} = \omega\frac{p_0 V_{c,0}}{\dot{m}_c a_0^2} \quad (8)$$

represents the ratio of the seal discharge time through the gap $t_d = p_0 V_{c,2D}/(\dot{m}_c a_0^2)$ and the vibration period of the seal, being a_0 the speed of sound. Unlike in the linear problem described in [12], the total inlet temperature and pressure are used to define Ω_{NL} instead the mean static pressure and temperature of the seal. In this context, the characteristic mass-flow is $\dot{m}_c = \gamma p_0 A_0/a_0$, where A_0 is the nominal clearance area that is deemed to be the same for both fins.

The mechanical to acoustic frequency ratio is defined as

$$St = \frac{\omega R}{ND\,a_0}. \quad (9)$$

where in the general case, $\omega = \omega(ND)$ and St can be expressed as a function of either the angular frequency, ω, or the nodal diameter, ND.

The model assumes that the seal mode-shape can be represented as a rigid body motion about a pivot point in the meridional section (see Fig. 1). Therefore, the dimensionless gap and volume time variations can be expressed as function of the distance between the pivot center and the inter-fin cavity center, r, considered positive if it is located in the LPS, the geometric parameters that define the seal L, s, and H_0 and the vibration amplitude, $\Delta\theta$, as:

$$\tilde{A}_{1,2} = 1 + \frac{r \pm L/2}{H_0}\Delta\theta\sin\tau, \text{ and } \tilde{V}_{c,2D} = 1 + \frac{r}{s}\Delta\theta\sin\tau. \quad (10)$$

Though it has been proved [14, 13] that the effect of the dissimilar gap on the stability can be large, for the sake of simplicity in this work a seal with identical gaps is considered, i.e. $H_1 = H_2$, and consequentlythe non-dimensional gap areas are the same, i.e. $\tilde{A}_1 = \tilde{A}_2$.

Linear Solution

This section summarizes the main results of the linearized model described in [12] to ease the comparison with the nonlinear results in the limit of small-amplitude clearance variation. The linear model has been compared in a wide range of operating conditions to 3D linearized Navier-Stokes solutions with excellent results [13, 14]. For this reason, it is expected that the equivalent one-dimensional nonlinear model compares well with 3D nonlinear Navier-Stokes solutions. However, this work is postponed to a future publication.

The linearized model is obtained assuming that the gap and volume variations are small, i.e. $A_j = A_{j,0} + a_j(t)$, and $V_c = V_{c,0} + v_c(t)$ with $a_j \ll A_{j,0}$ and $v_c \ll V_{c,0}$, and the flow perturbations in the inter-fin cavity associated with the seal vibration are small. In this case, the flow variables in inter-fin cavity can be decomposed as the sum of a mean or steady field, denoted with the sub-script s, plus a small perturbation,

$$\rho_c = \rho_{c,s} + \rho_c', \; p_c = p_{c,s} + p_c', v_\theta = v_{\theta,s} + v_\theta' \quad (11)$$

with $\rho'_c \ll \rho_{c,s}$, $p'_c \ll p_{c,s}$ and $v'_\theta \ll v_{\theta,s}$ The circumferential unsteady variations of the flow are retained in the model but the mean flow field is deemed spatially uniform. The unsteady perturbations are assumed to vary solely in the circumferential direction. The seal vibration is introduced imposing that the volume and gap variations of the seal have the form of traveling-waves. The resulting set of linearized equations is solved seeking traveling-wave solutions as well.

The dimensionless work-per-cycle is defined as

$$\tilde{W}_{cyc} = \frac{W_{cyc}}{\pi p_{c,s} \delta^2 SL/(rH_0 h')} \tag{12}$$

where $S = 2\pi RL$ is the surface of the seal bottom, $p_{c,s}$ the mean pressure of the inter-fin cavity, r the distance of the pivot point to the mid-point of the seal, and $\delta = r\Delta\theta$, the vibration amplitude of this point. The work–per-cycle carried out by the fin surfaces cancels out since the static pressure is deemed constant in the inter-fin cavity, and only the contribution of the bottom of the seal is considered. The actual expression of the dimensionless work-per-cycle is (see [12]):

$$\tilde{W}^{Lin}_{cyc} = -\bar{\Omega}\left[\tilde{e}h'_{eff} + \left(1 - \frac{1}{St^2}\right)\right] \Big/ \left[\tilde{1} + \bar{\Omega}^2 \left(1 - \frac{1}{St^2}\right)^2\right] \tag{13}$$

where h' is a involved function of the seal pressure ratio (see appendix A in [8]) that is modified taking into account non isentropic effects (see [12]) to obtain h'_{eff}. The dimensionless gap or torsion center

$$\tilde{e} = \frac{\gamma r H}{sL}. \tag{14}$$

groups the effect of the pivot center, r, the seal clearance, H, and the geometry of the seal (see Fig. 1). In the higher-order formulation, the two parameters $\tilde{e}$ and h'_{eff} appear always grouped as $\tilde{e}h'_{eff} = \tilde{e}h'F(\Omega)$ but if the perturbations are deemed isentropic, which is an accurate assumption in realistic cases, then $F(\Omega) = 1$.

The non-dimensional parameter $\bar{\Omega}$, is similar to that introduced in the nonlinear formulation (Eq. 8) and represents as well the ratio between the discharge time of the seal and the period of vibration. However, it differs due to two factors. In the linear non-isentropic formulation $\bar{\Omega} = \hat{\Omega}\tilde{\Omega}$, where $\hat{\Omega}$, is a function that varies smoothly between one and γ. In practical cases $\hat{\Omega} \simeq 1$ and $\bar{\Omega} = \Omega/h' = \tilde{\Omega}$, where

$$\Omega = \frac{\omega p_c V_{c,0}}{\dot{m}_s a_0^2}. \tag{15}$$

Even in this simpler case, $\Omega \neq \Omega_{NL}$ since the pressure in the cavity, p_c, and the mass flow, m_s, are unknown in the nonlinear formulation. These two variables have to be replaced in the non-dimensionalization process by p_0 and $\dot{m}_c$, that are known from the boundary conditions of the problem.

It is important to note that in this work the super-script tilde$\tilde{}$, is used for the non-dimensional variables, except for the non-dimensional discharge time, $\tilde{\Omega}$, where the super-script indicates that Ω has been scaled by a function of the total pressure ratio, h'. Under the same conditions (relatively high frequencies of vibration) the function $\tilde{1}$ of the expression 13 is close to one as well. The reader is referred to [12] for further details.

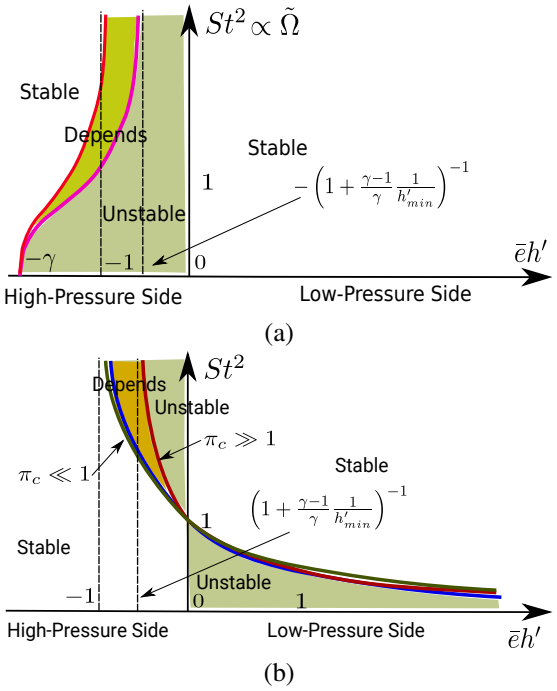

FIGURE 2. STABILITY REGION OF THE HIGHER-ORDER CV MODEL [12]. (A) THE 0^{th} NODAL DIAMETER STABILITY LIMIT AS A FUNCTION OF THE DIMENSIONLESS DISTANCE FROM THE PIVOT CENTER OF THE MODE TO THE SEAL MID-POINT ($\tilde{e}h'$) AND THE DIMENSIONLESS FREQUENCY ($\tilde{\Omega}$). (B) THE GENERAL STABILITY LIMIT INCLUDING THE CIRCUMFERENTIAL PERTURBATIONS, AS A FUNCTION OF THE DIMENSIONLESS DISTANCE FROM THE PIVOT CENTER OF THE MODE TO THE SEAL MID-POINT ($\tilde{e}h'$) AND THE MECHANICAL TO ACOUSTIC FREQUENCY RATIO (St).

Figure 2 summarises the stability criterion derived in [8, 12]. Figure 2(a) shows the stability limit for the 0th ND. Seals supported on the LPS ($\tilde{e}h' > 0$) are always stable. Instead, when the support is located on the HPS the seals are unstable if the pivot center is close to the seal. However, when the pivot center is located far away from the seal this is stable again. The stability on the HPS depends on the frequency ($\tilde{\Omega}$) and on the pressure ratio of the seal, because $\tilde{e}h'_{eff}$ is a function of Ω. The green area in Fig. 2 corresponds to unstable combinations of the torsion centre and the vibration frequency, whilst the orange region signals potentially unstable areas depending on the pressure ratio of the seal.

Figure 2(b) represents the general stability criterion, accounting for the circumferential perturbations. The seal is unstable for

TABLE 1. GEOMETRICAL PARAMETERS AND OPERATING CONDITIONS

$L\ [mm]$	$s\ [mm]$	$H\ [mm]$	$R\ [m]$	π_T
15.8	10.1	0.2	0.554	1.2

low vibration frequencies ($St \lesssim 1$) if the support is on the LPS. However, when the support is on the HPS the seal is unstable if the pivot point is close enough to the seal ($\tilde{e}h' < -1$) for high frequencies of vibration ($St \gtrsim 1$).

On the HPS, the stability limit depends on the pressure ratio across the cavity, $\pi_c = p_c/p_e$. Interestingly, the higher the pressure ratio, the larger the stability region on the HPS is. The separation line between the regions whose stability depends on π_c is signaled with the label $\pi_c \gg 1$ in Fig. 2 (b).

Numerical Model

The governing equations (Eq. 1) are integrated in time using a fourth-order Runge-Kutta for a prescribed harmonic motion until the solution converges to a periodic state. The spatial derivatives are discretised using second-order centred finite differences and periodic boundary conditions are used in the circumferential direction. A fourth order artificial dissipation term is included to damp high-frequency oscillations. The dimensionless set of governing equations 7 can be expressed as:

$$St\frac{\partial(\tilde{V}_c\tilde{\mathbf{U}})}{\partial\tau}+\frac{\partial(\tilde{V}_c\tilde{\mathbf{h}})}{\partial\tilde{z}}=\tilde{\mathbf{S}}-\mu_4|1+\tilde{v}_\theta|\Delta\tilde{z}^3\frac{\partial^4\tilde{\mathbf{U}}}{\partial\tilde{z}^4} \quad (16)$$

where $\tilde{\mathbf{S}}$ is a forcing term including the gap and the volume variation of the seal, and depending on dimensionless geometric factors (i.e. $\tilde{L},\tilde{r},r/s$), the vibration amplitude $\Delta\theta$, and two dimensionless flow parameters,

$$\tilde{\mathbf{S}}=\tilde{\mathbf{S}}(\tilde{\mathbf{U}},\tau,\Omega_{NL},\pi_T,\Delta\theta,\tilde{L},\tilde{r},r/s). \quad (17)$$

The last term on the right hand side of Eq. 16 represents the numerical diffusion. The work-per-cycle is extracted from the last cycle of the converged periodic solution.

The geometry used to explore the nonlinearity of the model has been used in previous works [14, 13] and is summarized in Tab. 1. It consists of a simply two-fin straight-through seal for which the linear model was able to reproduce the results obtained with a three-dimensional linearized Navier-Stokes solver [14].

RESULTS

Zero Nodal Diameter Case

The results of the nonlinear model for the 0th nodal diameter are described first. If the circumferential variations are neglected,

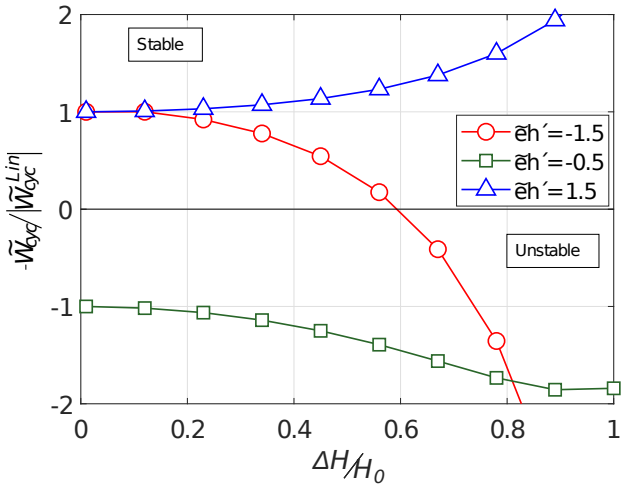

(a) $\Omega_{NL}=1.2$

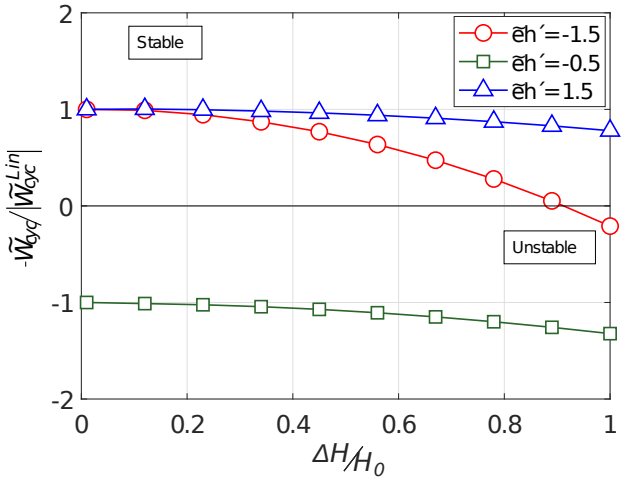

(b) $\Omega_{NL}=24$

FIGURE 3. DIMENSIONLESS WORK-PER-CYCLE NORMALIZED WITH THE WORK-PER-CYCLE OF THE LINEAR (SMALL AMPLITUDE) CASE AS A FUNCTION OF THE VIBRATION AMPLITUDE FOR DIFFERENT POSITIONS OF THE DIMENSIONLESS TORSION CENTER ($\tilde{e}h'$). THE TOTAL PRESSURE RATIO OF THE SEAL IS $\pi_T = P_0/p_e = 1.2$ AND THE CORRESPONDING $h' = 10.5$.

solely the mass and energy equations need to be solved, and the set of governing equations becomes a system of ordinary differential equations in time.In non-dimensional form the resulting equations reduce to:

$$\Omega_{NL}\frac{d}{d\tau}\left(\tilde{\rho}_c\tilde{V}_c\right)=\tilde{A}_1\left(\tau\right)g\left(\tilde{p}_c\right)-\tilde{A}_2\left(\tau\right)\tilde{p}_c^{1/2}\tilde{\rho}_c^{1/2}g\left(\tilde{p}_c\pi_T\right) \quad (18)$$

$$\Omega_{NL}\frac{d}{d\tau}\left(\tilde{p}_c\tilde{V}_c\right)=\gamma\tilde{A}_1\left(\tau\right)g\left(\tilde{p}_c\right)-\gamma\tilde{A}_2\left(\tau\right)\tilde{p}_c^{3/2}\tilde{\rho}_c^{-1/2}g\left(\tilde{p}_c\pi_T\right)-(\gamma-1)\Omega_{NL}\tilde{p}_c\frac{d\tilde{V}_c}{d\tau} \quad (19)$$

Figure 3 shows the variation of the dimensionless work-per-cycle of the seal, $\tilde{W}_{cyc}$, normalized with the small amplitude (linear) limit, $\tilde{W}_{cyc}^{Lin}$, obtained using Eq. 13, as a function of the vibration amplitude of the seal, $\Delta H/H_0$. When $\Delta H/H_0 = 1$, the tip of the seal fin rubs with the static part during a single instant of the vibration period. It is important to remark that ΔH is the vibration amplitude in the vertical direction of the fin tip located farther away from the pivot center. If the seal is supported on the LPS, this vibration amplitude corresponds to the tip of the inlet fin, whereas if the seal is supported on the HPS this amplitude is that of the exit fin. Two dimensionless frequencies $\Omega = 1.2$ and $\Omega = 24$ are presented, being the former too low for a realistic case while the latter is deemed realistic.

The first remark is that the quadratic dependence of work-per-cycle with the vibration amplitude that is obtained from the linear analysis, i.e. $W_{cyc}^{Lin} \propto \delta^2 \propto (\Delta H)^2$, is absorbed by the non-dimensionalization, so the variation of $\tilde{W}_{cyc}$ with the amplitude shown in Fig. 3 is due to higher-order terms. It can be observed that for the cases displayed here, the linear behavior holds as long as $\Delta H/H_0 \ll 1$ that is an expected result. In practice, for $\Delta H/H_0 \sim 0.2$, the seal behaves still linearly, but for higher values of the amplitude the seal can change its stability. Stable seals supported on the HPS ($\tilde{e}h' = -1.5$) can become unstable, instead, the opposite trend is observed for seemingly stable seals supported on the LPS, which become more stable when the clearance variation increases. The main conclusion is that nonlinearities can play a relevant role in the stability of the 0th ND.

Another important conclusion is that since the nonlinear correction to the work-per-cycle scales as δ^4, i.e. $W_{cyc} = W_{cyc}^{*,Lin}\delta^2 + W_{cyc}^{*,NL}\delta^4$ the dimensional W_{cyc} renormalized with the linear work-per-cycle is

$$\frac{W_{cyc}}{W_{cyc}^{Lin}} = 1 + \frac{W_{cyc}^{*,NL}}{W_{cyc}^{*,Lin}}\delta^2 \tag{20}$$

so the curves displayed in Fig. 3 are parabolas (at least for $\Delta H/H_0 \ll 1$).

The comparison of Figs. 3a and 3b for a seal is supported on the LPS ($\tilde{e}h' = +1.5$) leads to the conclusion that nonlinear effects are stronger at low frequencies than at high frequencies. This fact can be corroborated by looking at the static pressure time signals of the final periodic state displayed in Fig. 4. The unsteady pressure is renormalized with the linear estimate of the unsteady pressure derived in [8] where it was found that $p_c' = (p_c - p_{c,s}) \sim \varepsilon p_{c,s}$ with $\varepsilon = L\Delta\theta/(H_0 h')$, and which for small amplitudes is small necessarily.

Figure 4a shows that the closing and opening intervals of the seal behave in a completely different manner being the former highly nonlinear for large vibration amplitudes when Ω is low. The unsteady pressure amplitude grows higher than linear for high vibration amplitudes. Moreover, it can be noticed that the mean

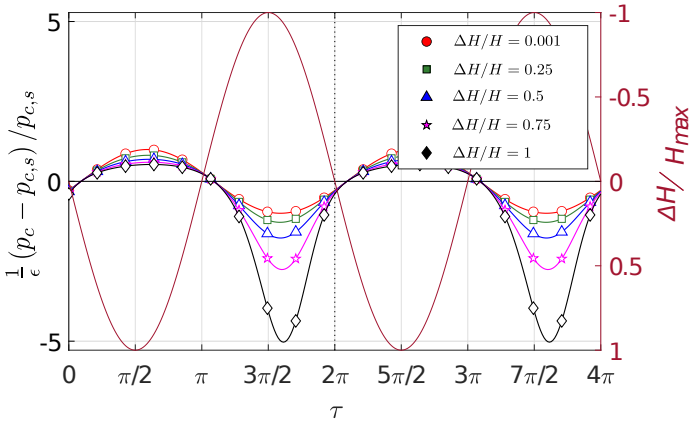

(a) $\Omega_{NL} = 1.2$

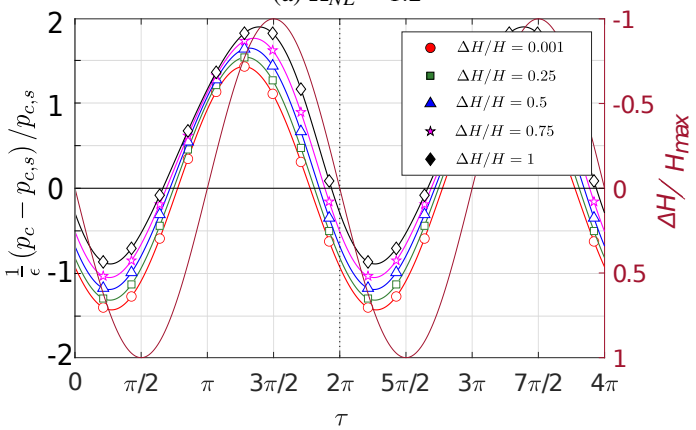

(b) $\Omega_{NL} = 24$

FIGURE 4. IMPACT OF THE VIBRATION AMPLITUDE ON THE UNSTEADY PRESSURE TIME SIGNAL FOR TWO DIFFERENT FREQUENCIES AND 5 VIBRATION AMPLITUDES FOR A SEAL SUPPORTED ON LPS ($\tilde{e}h' = +1.5$; $\pi_T = 1.2$; $h' = 10.5$). THE SOLID LINE WITHOUT SYMBOLS REPRESENTS THE DIMENSIONLESS VARIATION OF THE GAP.

value of the static pressure in the inter-fin cavity experiences a drift from the steady-state value due to nonlinear effects. This is another indication of the non-linearity of the problem. It can be observed that the pressure in the cavity is in anti-phase, in first approximation, with the radial displacement of the seal. This is a direct consequence of the relatively low frequency of the motion.

The situation is quite different at high-frequencies (precisely speaking $\Omega \gg 1$). Figure 4b shows that the unsteady pressure has a sinusoidal shape for $\Omega = 24$, which is a signal of the linearity of the problem. However, the mean pressure changes with the vibration amplitude. In this case, the static pressure in the cavity slightly lags the radial displacement of the seal.

The quasi-linear sinusoidal behaviour of the unsteady pressure is the result of two combined effects, namely the high frequency

and the fact that the volume variations of the inter-fin cavity are small compared to the volume. The dimensionless volume, $\tilde{V}_c = 1 + \tilde{v}_c \sin\tau$, where $\tilde{v}_c = \delta/s < H_0/s \ll 1$. The dimensionless mass and momentum equations are of the form

$$\frac{d}{d\tau}\left(\tilde{\rho}_c \tilde{V}_c\right) = \frac{1}{\Omega_{NL}} F_m\left(\tilde{\rho}_c, \tilde{p}_c, \tau\right) \simeq 0, \tag{21}$$

$$\frac{d}{d\tau}\left(\tilde{p}_c \tilde{V}_c\right) + (\gamma - 1)\,\tilde{p}_c \frac{d\tilde{V}_c}{d\tau} = \frac{1}{\Omega_{NL}} F_e\left(\tilde{\rho}_c, \tilde{p}_c, \tau\right) \simeq 0 \tag{22}$$

where F_m and F_e are nonlinear functions whose impact is negligible in first approximation if $\Omega_{NL} \gg 1$. The mass equation neglecting terms small terms of the form $\mathcal{O}(\tilde{v}_c)$ and $\mathcal{O}\left(\Omega_{NL}^{-1}\right)$ can be written as

$$\frac{d\tilde{\rho}_c}{d\tau} + \tilde{\rho}_c \tilde{v}_c \cos\tau \simeq 0 \tag{23}$$

whose periodic solution is $\tilde{\rho}_c/\tilde{\rho}_{c,s} = e^{-\tilde{v}_c \sin\tau} \simeq 1 - \tilde{v}_c \sin\tau$. Analogously, the energy equation reduces in first approximation to $\tilde{p}_c/\tilde{p}_{c,s} \simeq 1 - \gamma\tilde{v}_c \sin\tau$. Therefore, the unsteady perturbations at high frequency are isentropic, as it had already been observed in [12], and harmonic in first approximation. This is a clear indication that nonlinear effects are expected to be small at high frequencies.

General Case

Despite the 0th ND case being a simple introductory instrumental case to understand the implications of nonlinear effects on the stability, retaining the circumferential variations is essential to obtain meaningful results. It is important to note that in this section, the seal stability is assessed by evaluating the dimensionless work-per-cycle that is proportional to the square of the vibration amplitude. This means that the variations of the work-per-cycle with the vibration amplitude observed here are solely due to nonlinear effects. For a given geometry, pressure ratio across the seal, torsion center position, and frequency, the non-dimensional work-per-cycle is a function of four non-dimensional parameters only

$$\tilde{W}_{cyc} \equiv \tilde{W}_{cyc}\left(\Omega_{NL}, St, \tilde{e}h', \Delta H/H\right). \tag{24}$$

The effect of the nonlinearities on the stability is studied by using the geometry described in Tab. 1 for three torsion center positions, two located on the HPS, $\tilde{e}h' = -2$ and $\tilde{e}h' = -0.4$, and other located on the LPS $\tilde{e}h' = 1.5$. The three torsion centres were selected to cover the three different stability regions of the linear model (see Fig. 2(b)) The total pressure ratio of the seal is $\pi_T = P_0/p_e = 1.2$ and the corresponding $h' = 10.5$.

Figure 5 shows the variation of the non-dimensional work-per-cycle normalized with the work-per-cycle of the linear model as a function of the frequency ratio, St, with the support located far from the seal on the HPS, $\tilde{e}h' = -2$ ($r/L = -6.8$ in more physical terms). For small amplitudes, the seal is stable independently of the frequency, as described in Fig.2(b). However, for small

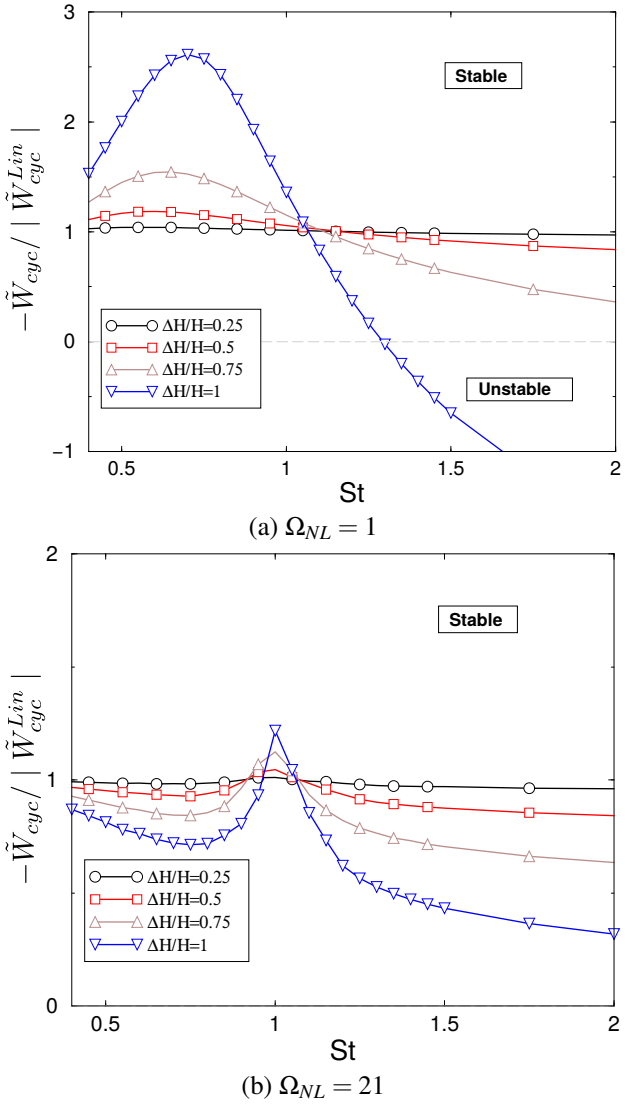

FIGURE 5. DIMENSIONLESS WORK-PER-CYCLE VARIATION NORMALIZED WITH THE WORK-PER-CYCLE OF THE LINEAR (SMALL AMPLITUDE) CASE FOR A SEAL SUPPORTED ON THE HPS, $\tilde{e}h' = -2$. THE NON-DIMENSIONAL WORK VARIATION IS EXPRESSED AS A FUNCTION OF THE FREQUENCY RATIO, St, FOR DIFFERENT VIBRATION AMPLITUDES, $\Delta H/H$. EFFECT OF THE NONLINEARITIES FOR A LOW NON-DIMENSIONAL FREQUENCY, $\Omega = 1$ (A) AND FOR HIGH NON-DIMENSIONAL FREQUENCY, $\Omega = 21$ (B).

non-dimensional frequencies (Ω_{NL}) the stability can change (see Fig.5,a). Instead, when the non-dimensional frequency is high (Fig.5,b) the seal is always stable independently of the vibration amplitude. Similar to the analytical model, a resonance is observed close to $St \simeq 1$ where the stability increases with the gap variation. The observed peak is the result of a small shift in the resonance frequency with respect to the linear case. Decreasing

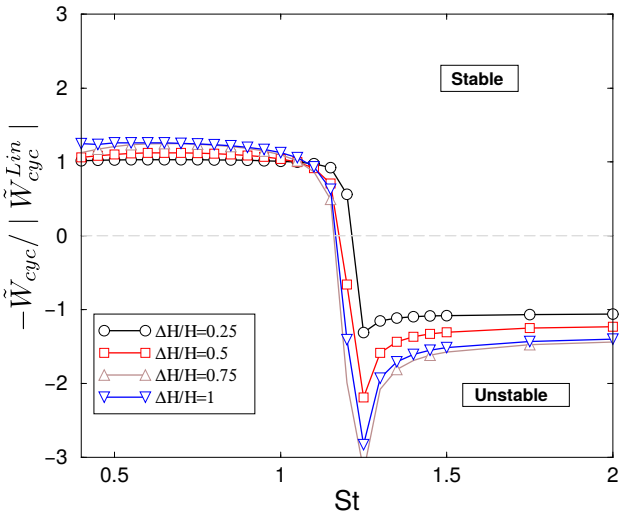

(a) $\Omega_{NL} = 1$

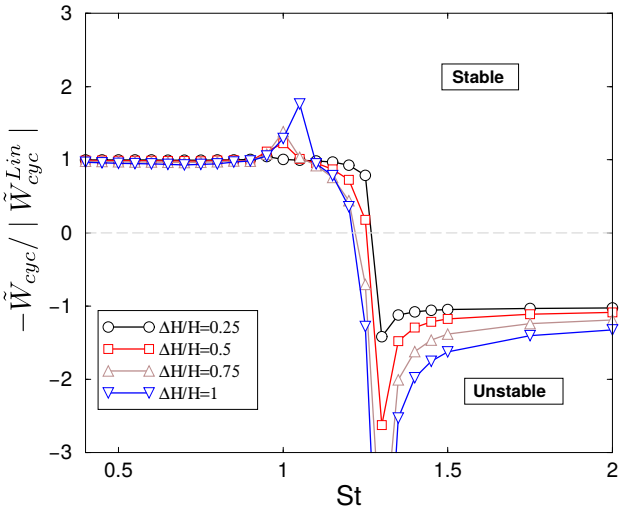

(b) $\Omega_{NL} = 21$

FIGURE 6. DIMENSIONLESS WORK-PER-CYCLE VARIATION NORMALIZED WITH THE WORK-PER-CYCLE OF THE LINEAR (SMALL AMPLITUDE) CASE FOR A SEAL SUPPORTED ON THE HPS, $\tilde{e}h' = -0.4$. THE NON-DIMENSIONAL WORK VARIATION IS EXPRESSED AS A FUNCTION OF THE FREQUENCY RATIO, St, FOR DIFFERENT VIBRATION AMPLITUDES, $\Delta H/H$. (A) EFFECT OF THE NONLINEARITIES FOR A LOW NON-DIMENSIONAL FREQUENCY, $\Omega = 1$ AND (B) FOR HIGH NON-DIMENSIONAL FREQUENCY, $\Omega = 21$.

the non-dimensional frequency, Ω, the resonance peak becomes smoother and lower, and moves to lower values of St.

Figure 6 shows the impact of the vibration amplitude on the dimensionless work-per-cycle, $\tilde{W}_{cyc}$, normalised with the solution of the linear model for a seal with the torsion center located close to the seal on the HPS, $\tilde{e}h' = -0.4$ ($r/L = -1.36$). In this case, the seal is unstable for $St > 1$ independently of the frequency, as described by the linear model (see Fig. 2b). The effect of the nonlinearities is marginal for the two non-dimensional frequencies tested and do not change qualitatively the behaviour of the seal. The typical resonance peak close to $St \simeq 1$ cannot be seen for low values of Ω (see Fig. 6a) independently of the clearance variation.This means that the linear model does a good absorbing the effect of the resonance.

Figure 6 should have ideally the form of a step function between one and minus one. Since the linear model predicts a change of stability, at a certain critical frequency ratio, St_c, the linear dimensionless work-per-cycle is null, $\tilde{W}^{Lin}_{cyc}(St_{cr}) = 0$, and the ratio $\tilde{W}_{cyc}/\left|\tilde{W}^{Lin}_{cyc}\right|$ is not well defined. The accurate numerical prediction of $\tilde{W}_{cyc}$ is difficult since the work-per-cycle is small and small errors in the phase can give rise to large errors in relative terms.

Figure 6b shows that for high values of the non-dimensional frequency, $\Omega \gg 1$, the linear stability limit is recovered when $St < 1$ even for the maximum vibration amplitude without contact with the casing ($\Delta H/H = 1$). The effect of the nonlinearities is more evident for high-frequency ratios, $St > 1$, leading to an increase of the work-per-cycle when the seal is unstable. The change in the critical frequency due to the effect of the vibration amplitude is about 10%.

Finally, Fig. 7 shows the impact of the vibration amplitude on the non-dimensional work-per-cycle normalized with the work-per-cycle of the linear case for a seal supported on the LPS, $\tilde{e}h' = 1.5$ ($r/L = 5.1$). As expected, the seal changes its stability for a frequency ratio less than one, $St < 1$. The support has been chosen far enough from the seal to magnify the sensitivity to the clearance variations, however, the effect of the nonlinearities is remarkable for low non-dimensional frequencies only. In fact, in Fig. 7a is apparent that the critical frequency ratio, St_{cr}, increases with the vibration amplitude extending the unstable behavior of the seal. On the other hand, for frequency ratios greater than one, $St > 1$, the seal is stable, and the high clearance variations increase the stability. For high values of the non-dimensional frequency (see Fig. 7b) the effect of the nonlinearities is limited, and the seal stability hardly departs from that predicted by the linear model for a wide range of vibration amplitudes. Similar to the case of low non-dimensional frequencies, the nonlinearities tend to reduce the stability of the seal by increasing the critical frequency ratio, St_{cr}.

Figure 8 shows the effect of the non-dimensional frequency on the stability for the maximum clearance variation, $\Delta H/H = 1$. The work-per-cycle is affected the most mostly when the support is located far away from the seal in the HPS (Fig. 8a). The nonlinear effects are stronger for low non-dimensional frequencies. In this case, the non-dimensional work-per-cycle can even change its sign when the frequency ratio is increased. Nevertheless, this scenario is not common in practical cases, where

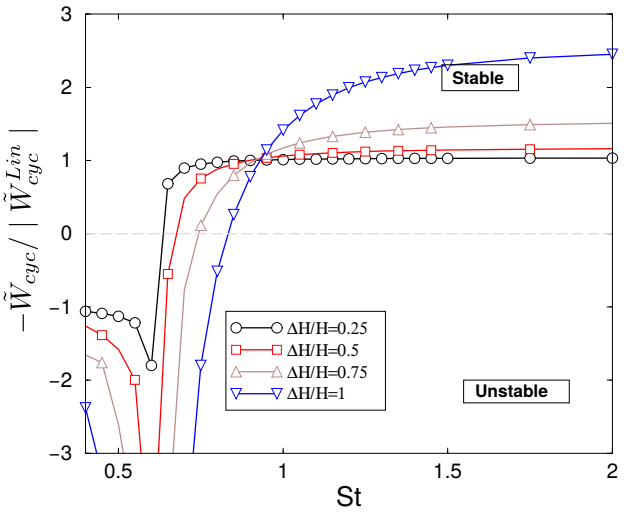

(a) $\Omega_{NL} = 1$

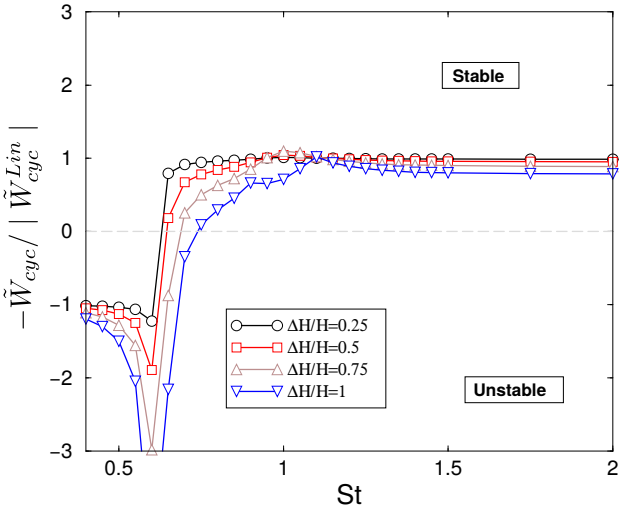

(b) $\Omega_{NL} = 21$

FIGURE 7. DIMENSIONLESS WORK-PER-CYCLE VARIATION NORMALIZED WITH THE WORK-PER-CYCLE OF THE LINEAR (SMALL AMPLITUDE) CASE FOR A SEAL SUPPORTED ON THE LPS, $\tilde{e}h' = 1.5$. THE NON-DIMENSIONAL WORK VARIATION IS EXPRESSED AS A FUNCTION OF THE FREQUENCY RATIO, St, FOR DIFFERENT VIBRATION AMPLITUDES, $\Delta H/H$. (A) EFFECT OF THE NONLINEARITIES FOR A LOW NON-DIMENSIONAL FREQUENCY, $\Omega = 1$ AND (B) FOR HIGH NON-DIMENSIONAL FREQUENCY, $\Omega = 21$.

the non-dimensional frequency is very high, $\Omega \gg 1$, and nonlinear effects barely affect the stability. The effect of the non-dimensional frequency on the stability when the support is located close to the seal in the HPS is shown in Fig. 8b. Similar to the linear analysis, the seal can be stable or unstable depending on the frequency ratio. The effect of very large clearance variations on the stability is very limited and the sensitivity on the frequency variation is low. The critical frequency ratio, St_{cr}, is hardly affected for the whole range of non-dimensional frequencies. Finally, Fig. 8c describes the effect of the non-dimensional frequency for a seal supported on the LPS. In general, increasing Ω the seal becomes more stable, and for realistic cases when $\Omega \gg 1$ the critical frequency ratio decreases.

Figure 9 shows the stability map for a two fin seal as described in Tab. 1 operating at a pressure ratio of $\pi_T = 1.2$ for a constant non-dimensional frequency, $\Omega_{NL} = 21$. The critical reduced frequency, St_{cr}, of the linear CV model [12] is obtained by imposing that $\tilde{W}^{Lin}_{cyc}(St_{cr}) = 0$ in Eq. (13), obtaining the following expression:

$$St^2_{cr} = \frac{1}{1 + \tilde{e}h'_{eff}(\Omega, h')} \tag{25}$$

and that corresponds to the solid and dashed lines plotted in the Fig. 9a and Fig. 9b, respectively. The dimensionless work-per-cycle is bounded between $-0.5 < \tilde{W}_{cyc} < 0.5$ to magnify the region where the stability change takes place. The main difference between the analytical linear model (Fig. 9a) and the nonlinear model (Fig. 9b) is that the unstable zone is larger in the later, both in the HPS and the LPS. When the support is located on the HPS the critical reduced frequency decreases, instead if the support of the seal is on the LPS the St_{cr} slightly increases. The unstable range would have been even wider if the discharge time of the seal had been close to the vibration period, as described in Fig. 8, however this limit is not deemed realistic. In practice, it can be safely said that labyrinth seals are more unstable at high vibration amplitudes.

CONCLUDING REMARKS

The nonlinear aeroelastic stability of labyrinth seals has been assessed extending the use of a well-verified linear model to the nonlinear regime. The expected accuracy of the results is high, based on the precedent validations of the linear model (see [12, 14, 13]) and the matching between the linear and nonlinear models at low vibration amplitudes.

The nonlinear stability has been studied first for a simplified case where all the meridional sections of the seal are moving in phase, the $0th$ ND case. The main conclusion is that in the presence of finite vibration amplitudes, the linear stability threshold is altered when the seal is supported on the high-pressure side whereas if the seal is supported on the low-pressure side, the seal is always stable. The vibration frequency plays a major role in the severity of nonlinear effects. Actually, for high enough vibration amplitudes, nonlinear effects are small even if the vibration amplitude of the seal is large and the seal closure becomes zero. This result is justified by simplifying the model for the high-frequency limit. Moreover, nonlinear effects are weakly affected by the seal pressure ratio.

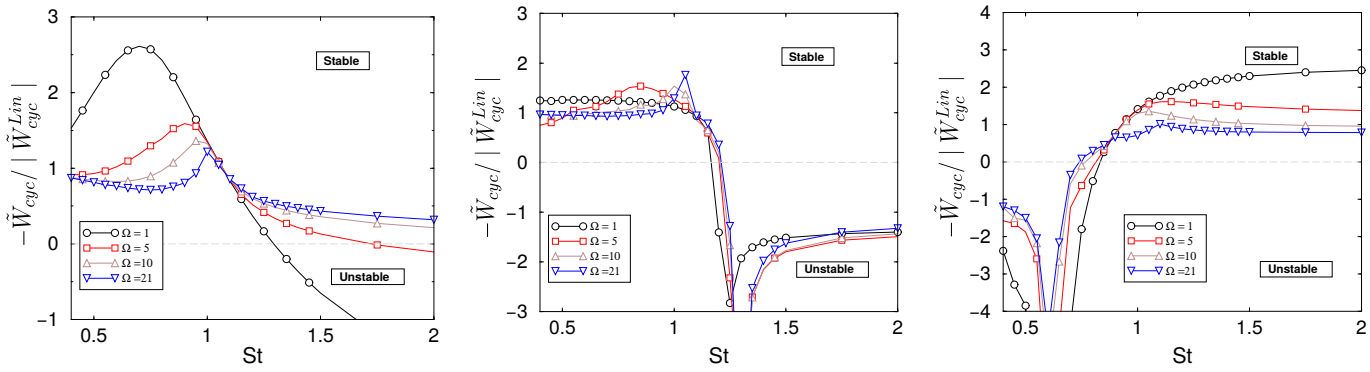

(a)$\tilde{e}h' = -2$ (b)$\tilde{e}h' = -0.4$ (c)$\tilde{e}h' = 1.5$

FIGURE 8. DIMENSIONLESS WORK-PER-CYCLE VARIATION NORMALIZED WITH THE WORK-PER-CYCLE OF THE LINEAR CV MODEL AS A FUNCTION OF THE FREQUENCY RATIO, St, FOR THE MAXIMUM CLEARANCE VARIATION, $\Delta H/H = 1$ AND FOR DIFFERENT NON-DIMENSIONAL FREQUENCIES, Ω. (A) SUPPORT ON THE HPS FAR FROM THE SEAL, $\tilde{e}h' = -2$, (B) SUPPORT ON THE HPS CLOSE TO THE SEAL, $\tilde{e}h' = -0.4$ AND (C) SUPPORT LOCATED ON THE LPS, $\tilde{e}h' = 1.5$.

When the azimuthal perturbations are included in the model, the stability decreases when the vibration amplitude is increased, except for values of the frequency ratio close to the resonance where the maximum stability is reached. This reduction of the stability can cause the change of the seal behavior if the support is on the HPS for values of $\tilde{e}h' < \gamma$, especially for low non-dimensional frequencies and for high values of the frequency ratio, $St \gg 1$. Even if this regime is of modest engineering interest since it is usually far away from the typical operating conditions of the seal, it shows for the first time that a stable seal can become unstable due to nonlinear effects. In realistic cases, where the discharge time of the inter-fin cavity is much longer than the vibration period, $\Omega \gg 1$, the nonlinear model shows that the nonlinear stability limit is close the linear stability threshold. Moreover, the critical frequency of the seal is sensitive to the nonlinear effects when the torsion center is located on the HPS. On the other hand, when the torsion center is on the LPS the reduction of the stability is limited (about 10% in terms of the critical frequency).

The present study shows that labyrinth seals are more unstable at large vibration amplitudes, and that the linear stability limit, even though close to the nonlinear one, is not conservative.

ACKNOWLEDGMENTS

This research work has been supported by the European project ARIAS, H2020 research and innovation program under grant agreement No. 769346. The authors gratefully acknowledge the financial support.

NOMENCLATURE

a_0	Speed of sound in the cavity
CV	Corral and Vega [8] Model
f, **h**	Convective fluxes
h'	Seal pressure function
H	Fin clearance
HPS	High-Pressure Side
ΔH	Clearance variation
$\tilde{e}$	$= \gamma \frac{rH}{sL}$, Non-dimensional torsion center
A_0	Nominal clearance area
v_θ	Azimuthal velocity
CFD	Computational Fluid Dynamics
$h_{0,i}$	Total enthalpy $h_{0,i} = c_p T_i + \frac{1}{2} v_i^2$
L	Seal cavity length
LPS	Low-Pressure Side
$\dot{m}$	Mass flow rate
ND	Nodal diameter
p_c	Cavity static pressure
p_e	Exit static pressure
P_0	Inlet total pressure
P_{c0}	Cavity effective total pressure
Q	Source term
r	Torsion center position
R	Cavity radius
s	Cavity height
St	$= \frac{\omega R}{ND\, a_0}$, Frequency ratio
t_d	$= \frac{p_{c,s} V_{c,s}}{\dot{m}_s a_0^2}$. Discharge time
$V_{c,2D}$	Seal volume per unit length

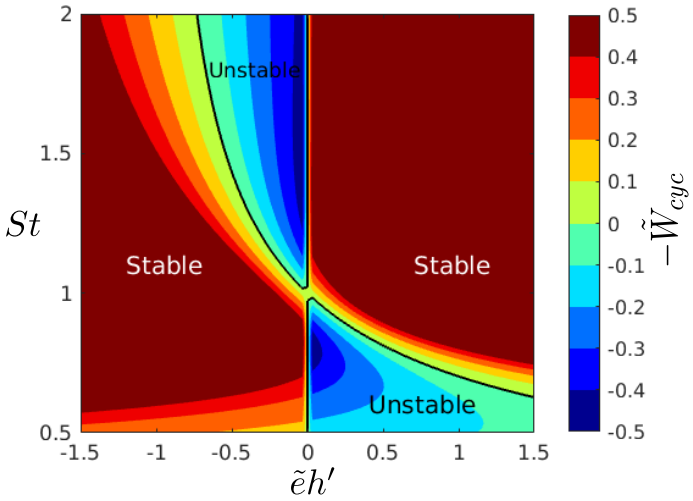

(a) Linear

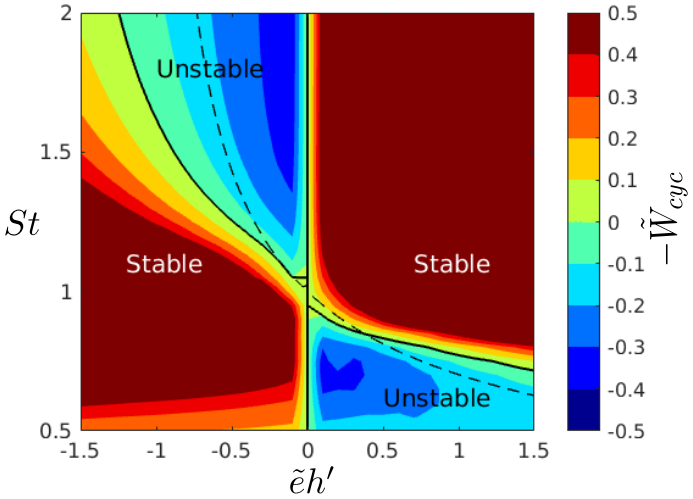

(b) Non-Linear

FIGURE 9. STABILITY MAPS ($\tilde{W}_{cyc}$) AS A FUNCTION OF THE DIMENSIONLESS TORSION CENTER, $\tilde{e}h'$, AND THE NATURAL-TO-ACOUSTIC FREQUENCY RATIO, St, FOR A PRESSURE RATIO OF $\pi_T = 1.2$ AND A NON-DIMENSIONAL FREQUENCY, $\Omega = 21$. (A) LINEAR MODEL FROM CORRAL ET AL. [12]. (B) STABILITY MAP FOR THE MAXIMUM CLEARANCE VARIATION, $\Delta H/H = 1$ CRITICAL FREQUENCY RATIO, SOLID LINES

W_{cyc}	Work per cycle
z	Azimuthal coordinate
Greek symbols	
γ	Heat capacity ratio
π	$= P_0/p_c$. Cavity pressure ratio
π_T	$= P_0/p_e$. Total pressure ratio
ω	Vibration angular frequency (rad/s)
Ω	$=\omega t_d$ Non-dimensional discharge time
$\tilde{\Omega}$	$=\Omega/h'$ Convenient form of Ω
$\bar{\Omega}$	$= \hat{\Omega}\tilde{\Omega}$, General form of Ω
$\Delta\theta$	Rotation angle
τ	Non-dimensional time
δ	$= r\Delta\theta$ Seal displacement
Super-scripts	
$\tilde{}$	Non-dimensional values
$\hat{}$	Normalized values
$'$	Time perturbation
Sub-scripts	
1	Inlet
2	Exit
c	Cavity
cyc	cycle
s	Steady state

References

[1] Hodkinson, B., 1939. "Estimation of the leakage through a labyrinth gland". *Proceedings of the Institution of Mechanical Engineers,* **141**, pp. 283–288.

[2] Alford, J., 1964. "Protection of labyrinth seals from flexural vibration". *ASME J. Eng. Gas Turbines Power,* **86**(2), October, pp. 141–147.

[3] Alford, J., 1967. "Protecting turbomachinery from unstable and oscillatory flows". *ASME J. Eng. Gas Turbines Power,* **89**, pp. 513–528.

[4] Alford, J. S., 1971. "Labyrinth seal designs have benefitted from development and service experience". In SAE Technical Paper, SAE International.

[5] Lewis, D., Platt, C., and Smith, E., 1979. "Aeroelastic instability in F100 labyrinth air seals". *AIAA Journal of Aircraft,* **16**(7), pp. 484–490.

[6] Ehrich, F., 1968. "Aeroelastic instability in labyrinth seals". *ASME J. Eng. Gas Turbines Power,* **90**(4), October, pp. 369–374.

[7] Abbot, D. R., 1981. "Advances in labyrinth seal aeroelastic instability prediction and prevention". *ASME J. Eng. Gas Turbines Power,* **103**(2), April, pp. 308–312.

[8] Corral, R., and Vega, A., 2018. "Conceptual flutter analysis of labyrinth seals using analytical models. part I: Theoretical background". *ASME J. Turbomach.,* **140**(10), October, p. 121006.

[9] Vega, A., and Corral, R., 2018. "Conceptual flutter analysis of labyrinth seals using analytical models. Part II: Physical interpretation". *ASME J. Turbomach.,* **140**(10), October, p. 121007.

[10] Corral, R., Vega, A., and Greco, M., 2020. "Conceptual flutter analysis of stepped seals". *ASME J. Eng. Gas Turbines Power,* **142**(7), July, p. 071001.

[11] Corral, R., Greco, M., and Vega, A., 2019. "Tip-shroud labyrinth seal impact on the flutter stability of turbine rotor blades". *ASME J. of Turbomachinery,* **141**(10), October, p. 101006.
[12] Corral, R., Greco, M., and Vega, A., 2021. "Higher-order conceptual model for seal flutter". *ASME J. of Turbomachinery,* **143**(7), July, p. 071006.
[13] Corral, R., Greco, M., and Vega, A., 2022. "Effective clearance and differential gapping impact on seal flutter modelling and validation". *ASME J. Turbomach.,* **144**(7), p. 071010.
[14] Greco, M., and Corral, R., 2021. "Numerical validation of an analytical seal flutter model". *Journal of the Global Power and Propulsion Society,* **5**, pp. 191–201.